

Large Single-Crystal Cu Foils with High-Index Facets by Strain-Engineered Anomalous Grain Growth

Yanglizhi Li, Luzhao Sun, Zhenghua Chang, Haiyang Liu, Yuechen Wang, Yu Liang, Buhang Chen, Qingjie Ding, Zhenyong Zhao, Ruoyu Wang, Yujie Wei,* Hailin Peng,* Li Lin,* and Zhongfan Liu*

The rich and complex arrangements of metal atoms in high-index metal facets afford appealing physical and chemical properties, which attracts extensive research interest in material science for the applications in catalysis and surface chemistry. However, it is still a challenge to prepare large-area high-index single crystals in a controllable and cost-efficient manner. Herein, entire commercially available decimeter-sized polycrystalline Cu foils are successfully transformed into single crystals with a series of high-index facets, relying on a strain-engineered anomalous grain growth technique. The introduction of a moderate thermal-contact stress upon the Cu foil during the annealing leads to the formation of high-index grains dominated by the thermal strain of the Cu foils, rather than the (111) surface driven by the surface energy. Besides, the designed static gradient of the temperature enables the as-formed high-index grain seed to expand throughout the entire Cu foil. The as-received high-index Cu foils can serve as the templates for producing high-index single-crystal Cu-based alloys. This work provides an appealing material basis for the epitaxial growth of 2D materials, and the applications that require the unique surface structures of high-index metal foils and their alloys.

High-index facets of metals, in which there is at least one Miller indices greater than unity, have attracted growing interest in fundamental research and technical applications. In comparison with the basal facets, i.e., (111), (100), and (110),

the presence of high-density of low-coordinated atoms, including the steps, edges, and kinks, endow high-index facets rich physical and chemical properties.^[1] For instance, the high-index Cu foil is an ideal electrode for the CO₂ electrochemical reduction reaction with high chemical selectivity and reactivity, because of its unique surface structures.^[2–4] Furthermore, high-index Cu surfaces, with special symmetries and surface states, provide a promising platform for the epitaxial growth of 2D materials, such as graphene and hexagonal boron nitride.^[5–10] To obtain high-index Cu single crystals, mechanical cutting of bulk Cu single crystals,^[11,12] and epitaxial deposition of Cu films on single-crystal inorganic substrates^[3,13,14] are mainly employed, though these approaches remain hindered by the limited size and index choice.

Recently, the annealing of polycrystalline Cu foils was reported to be a promising approach for producing large-area single-crystal Cu foils relying on the anomalous grain growth,^[15,16] since the rolled Cu foils can be produced in large quantities in a low-cost manner. However, driven by the surface energy, anomalous grain growth

Y. L. Z. Li, L. Z. Sun, H. Y. Liu, Y. C. Wang, R. Y. Wang, Prof. H. L. Peng, Prof. Z. F. Liu
Center for Nanochemistry
Beijing Science and Engineering Center for Nanocarbons,
Beijing National Laboratory for Molecular Sciences, College of Chemistry
and Molecular Engineering
Peking University
Beijing 100871, P. R. China
E-mail: hlpeng@pku.edu.cn; zfliu@pku.edu.cn


Y. L. Z. Li, L. Z. Sun, Y. C. Wang
Academy for Advanced Interdisciplinary Studies
Peking University
Beijing 100871, P. R. China

Y. L. Z. Li, L. Z. Sun, H. Y. Liu, Y. C. Wang, Y. Liang, B. H. Chen, Q. J. Ding,
Z. Y. Zhao, R. Y. Wang, Prof. H. L. Peng, Prof. Z. F. Liu
Beijing Graphene Institute
Beijing 100095, P. R. China

Z. H. Chang, Prof. Y. J. Wei
LNM, Institute of Mechanics
Chinese Academy of Sciences
Beijing 100190, P. R. China
E-mail: yujie_wei@lnm.imech.ac.cn

Z. H. Chang, Prof. Y. J. Wei
School of Engineering Sciences
University of Chinese Academy of Sciences
Beijing 100049, P. R. China

Dr. L. Lin
School of Physics and Astronomy
University of Manchester
Manchester M13 9PL, UK
E-mail: li.lin-2@manchester.ac.uk

 The ORCID identification number(s) for the author(s) of this article can be found under <https://doi.org/10.1002/adma.202002034>.

DOI: 10.1002/adma.202002034

usually prefers energetically the formation of Cu(111) with the minimum of surface energy. Thus, it remains a challenge to obtain single-crystal Cu foils with various sets of high-index facets.^[16,17]

In this study, instead of the surface energy, it was found that two dominate factors, strain energy and interface energy, were efficient in engineering the crystallographic orientation of Cu foils. Relying on the thermal-stress between Cu foil and its graphite susceptor during the annealing, we developed a strain-engineered anomalous grain growth technique to successfully batch-convert decimetre-sized polycrystalline Cu foils into Cu single crystals with a series of high-index facets. Density functional theory (DFT) calculations and molecular dynamics (MD) simulations were employed to confirm the contribution of strain energy to the formation of high-index grains. The as-prepared Cu foils are also applicable to the production of large-area high-index Cu/Ni alloy single crystals and to growth of high-quality 2D materials.

During the annealing process, if there is no interaction between the Cu foil and the susceptor, for instance, the typical contact-free annealing, the surface energy would become the major driving force in the formation of the Cu(111)-oriented grains during the annealing of Cu foil, because of the minimum surface energy of Cu(111) among all the crystal orientations (Route I, Figure 1a).^[16] In contrast, the contact between the Cu foil and the underlying susceptor means that the strain energy and interfacial energy should be also considered as

the driving forces in determining the orientation of anomalous grains. Note that because the excess of interfacial contact stress would limit the growth of large grain,^[16] graphite, with a moderate thermal expansion coefficient and ideal interfacial interaction with Cu foils, was chosen as the susceptor material (Experimental Section).^[18] The contact of Cu foil with the graphite susceptor and subsequent annealing enabled the formation of the Cu anomalous grain with a high-index facet (Route II, Figure 1a). To promote the continuous growth of as-received high-index Cu grain, a static gradient of temperature was carefully set during the annealing process (Note S1 and Figure S1, Supporting Information).^[15] As a result, decimeter-sized single-crystal Cu foils with various high-index facets were obtained in batches in spite of their relatively high surface energy. After the oxidation of the as-obtained Cu foils at 180 °C for 2–5 min, the boundaries between polycrystalline regions and single crystalline regions can be clearly visible by naked eyes, because of their different oxidation rates (Figure 1b; and Figure S2, Supporting Information).^[19]

Electron backscatter diffraction (EBSD) measurements were conducted on as-obtained high-index Cu foils to accurately determine their crystalline orientation. The distinct colors of the inverse pole figure (IPF) maps in the normal direction verify the successful production of single-crystal Cu foils with a library of crystal orientations (Figure 1c; and Figure S3, Supporting Information). The atomic force microscopy (AFM) was employed to probe the surface of as-obtained high-index Cu

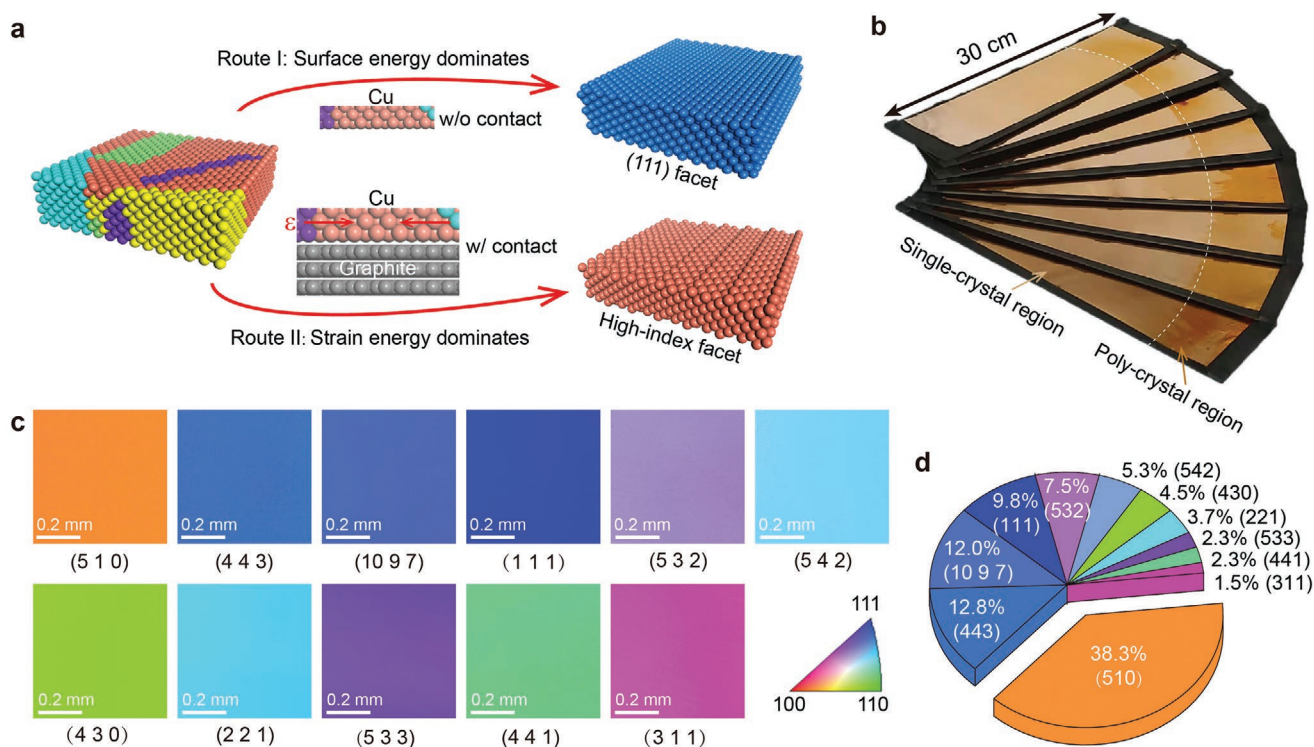


Figure 1. Strain-engineered annealing for growing large-area single-crystal Cu foils with high-index facets. a) Schematics of anomalous grain growth of Cu foils during the annealing without (route I) and with (route II) the contact with susceptor, respectively. b) Photograph of the batch-transformed high-index Cu foils on graphite susceptors. c) EBSD IPF maps of the as-prepared single-crystal Cu foils, with normal crystal orientation of (510), (443), (10 9 7), (111), (532), (542), (430), (221), (533), (441), (311), respectively. d) Pie chart of the proportions of facets in 133 pieces of as-obtained single-crystal Cu foils.

foils. The angles between slip lines on high-index Cu surface in AFM images were consistent with the theoretically calculated values, further confirming the crystalline orientation of as-received Cu high-index facets (Figure S4 and Table S1, Supporting Information).^[20] The statistics of crystal orientations of 133 pieces of as-obtained single-crystal Cu foils shows that (510) facet was the most frequently obtained crystal plane in general, followed by (443) facet and (10 9 7) facet (Figure 1d). The probability of obtaining rigid (111) plane is only 9.8%. Meanwhile, (110) vicinal surface, such as (430) and (441) facets were relatively rare, while other high-index crystal facets, such as (532) and (542) were also obtained with the probability of 7.5% and 5.3%, respectively.

As the most favorable high-index facet, we further characterized the crystal orientation of as-received Cu(510) on a large scale. Figure 2a displays a photograph of a large-scale (over 100 cm²) single crystal Cu(510) foil, where the homogeneous color after the oxidation indicates the formation of large-area single crystal on macroscale. The slip lines were clearly observed with an included angle of $\approx 80^\circ$ in the AFM image of Cu(510) crystal (Figure 2b), consistent with the theoretical value (80.7°) according to the (510) orientation (Table S1, Supporting Information). To test the crystal orientation both in the normal direction and in-plane direction, EBSD measurements were conducted on the five different regions marked in Figure 2a. The IPF color maps in normal direction show uniform orange color, which agrees well with the characteristics of the (510)

facet (Figure 2c). The identical distribution of projection points in the (001) pole figures manifests the same in-plane crystal orientation (Figure 2d). Furthermore, the high consistency of surface orientation was confirmed by a small angular variation (less than 1°) in the kernel average misorientation (KAM) maps (Figure 2e). All the above observations confirm the successful preparation of a high-quality single-crystal Cu foil with high-index (510) facet.

To better understand the formation of colossal high-index single crystal, the anomalous grain growth during the strain-engineered annealing was carefully investigated by using the theory of grain boundary (GB) migration (Note S2, Supporting Information), and the single-crystallization process is illustrated in Figure S5, Supporting Information. The migration rate (v) of Cu GB is proportional to the driving force P in the form of following equation^[21]

$$v = m \cdot P \quad (1)$$

where m is the mobility of Cu GB, associated with the atomic structure of the GB and external factors, such as temperature. The driving force P arises from the Gibbs free energy minimization (Figure S6, Supporting Information).^[21] For a supported thin film by a susceptor, there are three driving forces for GB migration: the surface energy (γ_s), the interface energy (γ_i) induced by the contact between film and substrate, and the strain energy (with a density of w) induced by thermal

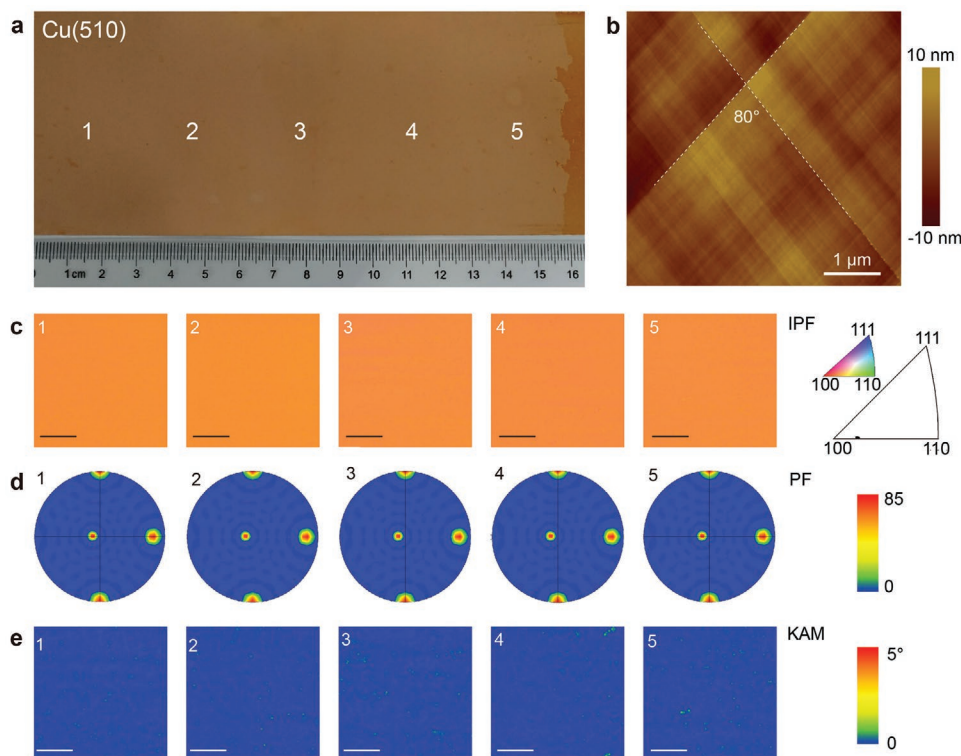


Figure 2. A large-area Cu(510) foil produced by strain-engineered annealing method. a) Photograph of the as-obtained large-area Cu(510) foil after the mild-oxidation. b) AFM image of as-obtained Cu(510) foil. White spotted lines denote the slip lines. c–e) EBSD IPF maps in the normal direction (c), (001) pole figures (d), and KAM maps (e) of the as-obtained Cu(510) foil collected at the corresponding positions marked in (a). Scale bars: 35 μm .

mismatch.^[22,23] Thus, the free energy density of a single grain (G) can be then approximated according to the following equation

$$G = \frac{\gamma_s}{h} + \frac{\gamma_i}{h} + w \quad (2)$$

where h is the thickness of the Cu foil, 50 μm in our case. The small thickness of Cu foil, compared to the other dimensions, means that the Cu foil is under a plane stress state, and we assume the stress is biaxial. Thus, the strain energy density (w) can be given according to the following equation^[24]

$$w = M_{hkl} \varepsilon^2 \quad (3)$$

where M_{hkl} is the biaxial modulus of the grain with an (hkl) facet, and ε is the thermal strain arising from the interfacial contact stress between the Cu foil and susceptor (Note S3, Supporting Information). Therefore, γ_s , γ_i , M_{hkl} , and ε are determining factors of the driving pressure P for the grain growth.

Here, we calculated γ_s and γ_i of the basal facets ((111), (110), and (100)), and the high-index (510) facet by MD simulations (Note S4 and Figure S7, Supporting Information), as shown in Figure 3a,b, respectively, in which the (111) facet has the lowest

γ_s and γ_i . In contrast, Figure 3c shows the corresponding biaxial modulus of these crystal facets, demonstrating that M_{100} and M_{510} are clearly lower than M_{111} . In another word, (100) and (510) show lower strain energy density under a certain load.

Hence, the total free energy density (G) of Cu(111), Cu(110), Cu(100), and Cu(510) as functions of strain (ε), are calculated by combining Equations (2) and (3), and is shown in Figure 3d (detailed calculated values of γ_s , γ_i , and w in different crystal facets refer to Figure S8, Supporting Information). Clearly, if ε exceeds a certain value (around 0.02%), the strain energy difference would become the driving force in the free energy minimization, and favor the formation of grains with (100) vicinal facets, such as Cu(100) and Cu(510). Note that, the cold rolled polycrystalline Cu foils in our case usually exhibit a (100)-oriented cube texture with a high density of low-angle GBs around (100) grains during the heat treatment (Figure S9, Supporting Information).^[25,26] In the annealing process, the density of low-angle GBs would be enhanced before the anomalous grain growth (Figure S10, Supporting Information). In this case, because of its low mobility, GBs would hinder the continuous expansion of rigid (100) grains, which would be in turn consumed by other dominating facets according to the kinetics of anomalous grain growth.^[21] Therefore, with a relatively low strain energy, the (510) facet becomes the preferable facet

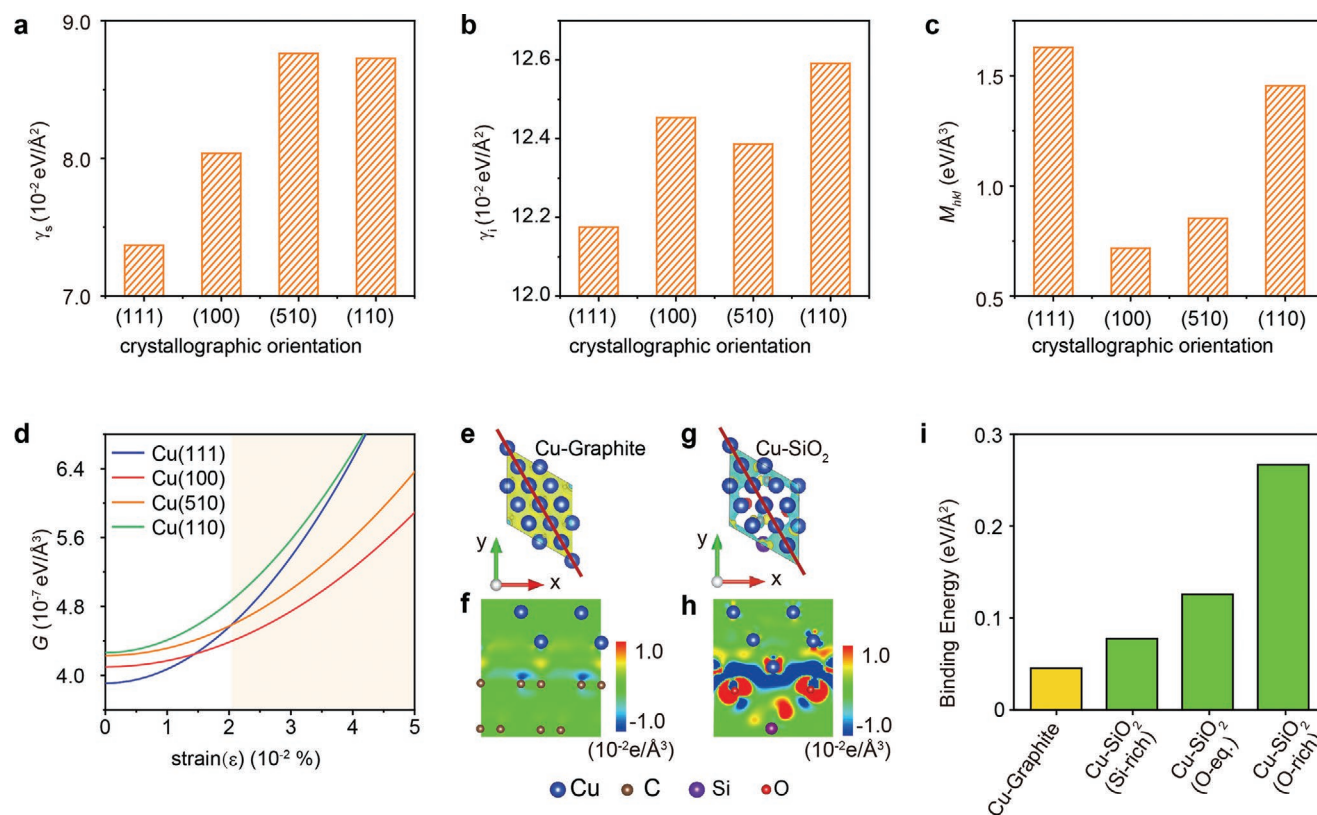


Figure 3. Theoretical calculations of the preference of crystal orientation in the strain-engineering annealing. a–c) Histogram of calculated surface energy (γ_s) of Cu (a), interface energy (γ_i) between Cu and graphite (b), and biaxial moduli (M_{hkl}) of Cu (c) with different facets. d) Free energy density (G) as functions of elastic strain. e, f) DFT-calculated charge densities of Cu on graphite: e) top view and f) cross-sectional view along the red line in (e). g, h) DFT-calculated charge densities of Cu on quartz (with an oxygen-rich surface): g) top view and h) cross-sectional view along the red line in (g). i) Calculated binding energies between Cu and graphite, and between Cu and SiO₂ with silicon-rich (Si-rich), silicon-oxygen-equal (O-eq.), and oxygen-rich (O-rich) surfaces, respectively.

thermodynamically and kinetically. Due to the high surface energy and strain energy density, the formation of (110) vicinal facets is difficult, which agrees well with our experimental results shown in Figure 1d.

The thermal stress between the Cu foil and the susceptor should be carefully controlled, to avoid strong plastic deformation in the Cu foil, which would make the strain density difference insufficient to drive the migration of GB.^[27] In addition, excess thermal stress would also crimp the Cu foil during the annealing. The choice of susceptor materials is essential for providing a suitable interfacial stress. Here, the binding energies of Cu-Graphite (corresponding to a graphite susceptor) and Cu-SiO₂ (corresponding to a typical oxide susceptor, such as quartz) systems were calculated based on DFT (Note S5, Supporting Information). As shown in Figure 3e,f, negligible charge transfer occurs between Cu and C atoms of the graphite susceptor since the interfacial interaction between the Cu foil and graphite is in the nature of Van der Waals. In contrast, Cu and O atoms in the Cu-SiO₂ system form a strong chemical bonding, giving rise to substantial charge transfer and a high binding energy (Figure 3g,h; and Figure S11, Supporting Information). The binding energies of Cu with graphite and quartz susceptors are summarized in Figure 3i. The strong binding between the SiO₂ susceptor and Cu foil would result in an

excess of interfacial stress and additional strain in Cu foils, hindering the colossal growth of the Cu grain, which is also consistent with previously reported observations (Figure S12, Supporting Information).^[16] Note that, the thermal stress is also influenced by the annealing temperature, thus tuning the annealing temperature might be powerful to endow the unique features (such as crystal orientation, phase, etc.) to other metals with high melting point.

The as-obtained single-crystal Cu foils with high-index facets can be further used as templates for producing single-crystal Cu-based alloy. For a vivid demonstration, we electroplated Ni films on as-obtained large-area Cu(510) and Cu(773) foils, respectively, and then annealed these layered structures at 1040 °C to form Cu₉₅/Ni₅(510) and Cu₈₅/Ni₁₅(773) (Figure 4a and the Experimental Section for details).^[28,29] The as-obtained large-area Cu₉₅/Ni₅(510) and Cu₈₅/Ni₁₅(773) foils both show an even optical contrast, indicating the high uniformity after the alloying process (Figure 4b,c). The colors of EBSD IPF maps are consistent with feature of (510) and (773) facets (Figure 4d,e; and Figure S13, Supporting Information). The included angles of slip lines shown in AFM images (Figure 4f,g) match well with the theoretical values shown in Table S1 of the Supporting Information. Thus, the above observations verified that the crystal orientation of Cu/Ni alloy is determined by that of the

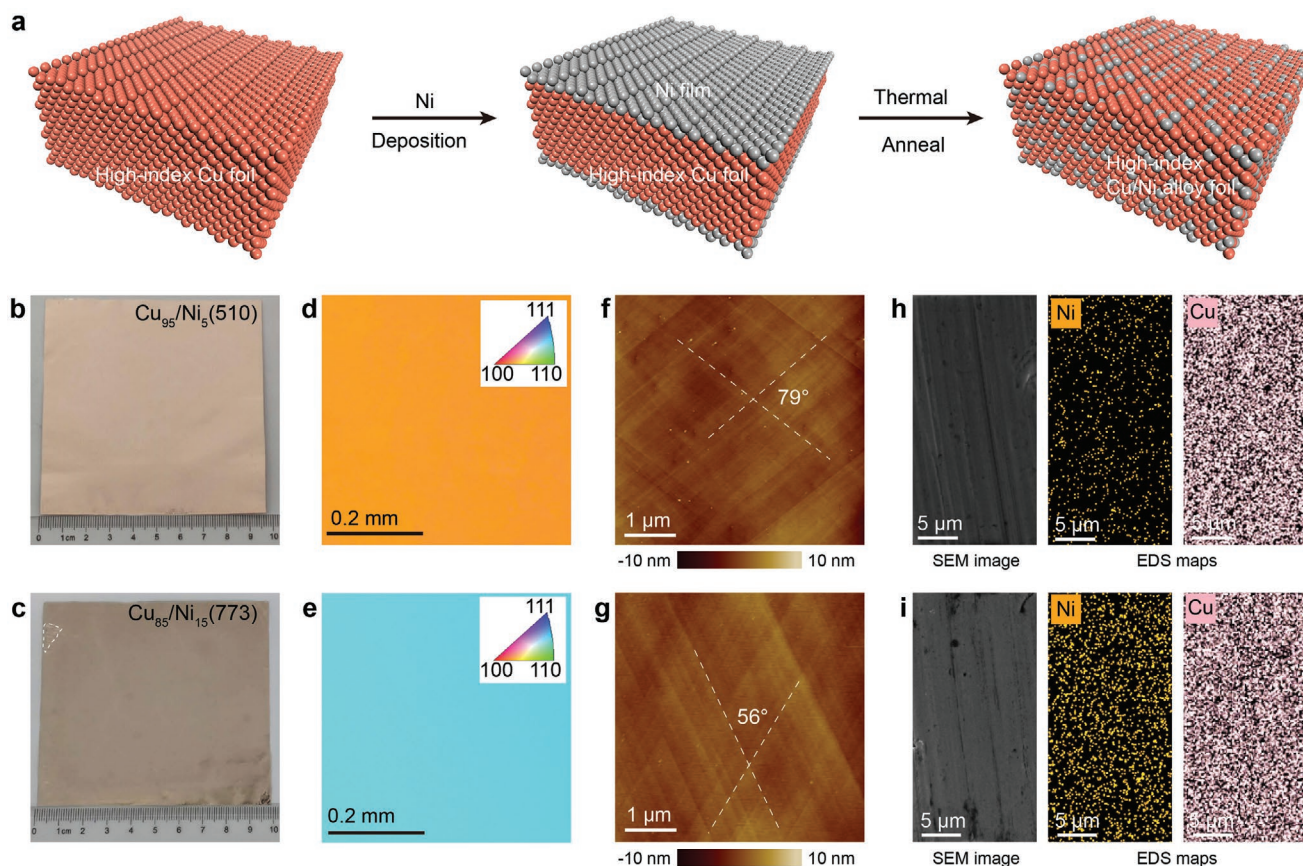


Figure 4. Preparation of high-index single-crystal Cu/Ni alloy foils by using the high-index Cu single crystal as templates. a) Schematic of preparing high-index single-crystal Cu/Ni alloy. b,c) Photographs of as-prepared single-crystal Cu₉₅/Ni₅(510) (b) and Cu₈₅/Ni₁₅(773) foils (c). d,e) EBSD IPF maps of Cu₉₅/Ni₅(510) foils (d) and Cu₈₅/Ni₁₅(773) foil (e). f,g) AFM images of Cu₉₅/Ni₅(510) (f) and Cu₈₅/Ni₁₅(773) (g). h,i) Cross-sectional SEM images and corresponding EDS maps of Cu₉₅/Ni₅(510) (h) and Cu₈₅/Ni₁₅(773) (i) foils.

original high-index Cu foil. The uniform distribution of Ni in the as-obtained Cu/Ni alloy foils was further confirmed by cross-sectional scanning electron microscopy (SEM), scanning transmission electron microscopy (STEM), and corresponding energy dispersive spectrum (EDS) mapping (Figure 4h,i; and Figure S14, Supporting Information), which suggest the diffusion and mutual fusion of Ni and Cu atoms are complete to form homogenous single-crystal Cu/Ni alloy.

Relying on the as-obtained single-crystal Cu foil with high-index facet, the epitaxial growth of aligned graphene was achieved with high-quality (Figure S15, Supporting Information). It is also possible to realize oriented growth of hexagonal boron nitride on some of the suitable high-index facets.^[30] Furthermore, high-index Cu facets consisting of (100) terrace and (110) or (111) steps show excellent selectivity toward ethylene for electrochemical CO₂ reduction.^[2]

In conclusion, a strain-engineered anomalous grain growth technique was developed to successfully prepare decimeter-sized single-crystal Cu foils with a library of high-index facets. DFT calculations and MD simulations revealed that strain energy plays a dominating role in determining the facets of Cu grains, enabling the preparation of high-index single-crystal Cu foils. Furthermore, large-area single-crystal Cu/Ni alloys can be prepared by using the single-crystal copper foils as templates. The availability of high-index metal single crystals with unique surface atomic arrangement by our approach would certainly bring us one step closer to the fundamental investigation of the novel properties and the fascinating applications of high-index metal foil, such as revealing the structure-activity relationship and enhancing the catalytic performance in model catalysis.

Experimental Section

Preparation of Single-Crystal Copper Foils: Commercially available copper foils (50 μm, Kunshan luzhifa Electronic Technology Co., Ltd) were attached to the graphite susceptors (SGL Carbon, R6710, Germany) and then inserted into the annealing furnace (Tianjin Zhonghuan Furnace Corporation, SK-G15123K-3-940). The temperatures of different heating zones were arisen from room temperature to target temperature, for example, 1030 °C (heating zone 1) and 1000 °C (heating zone 2) in 45 min and kept for 2 h to enable the anomalous grain growth. The annealing processes were conducted with 500 sccm H₂ and 100 sccm Ar. Finally, the Cu foils were cooled to room temperature for further characterization.

Preparation of Single-Crystal Cu/Ni Alloy Foils: As-prepared single-crystal Cu foils were electrochemically polished with a current density of ≈0.02 A cm⁻², which can reduce the surface roughness and impurities. Then, a layer of nickel film was deposited onto the surface of the copper foil by electroplating at a rate of ≈200 nm min⁻¹. The polishing solution was a mixture of 750 mL of orthophosphoric acid and 250 mL of glycol and the electrolytic solution was prepared by dissolving 280 g of NiSO₄·6H₂O, 8 g of NiCl₂·6H₂O, 4 g of NaF, and 30 g of H₃BO₃ in 1 L of deionized water. After washing and drying, the nickel-coated copper foils were loaded into a chemical vapor deposition (CVD) system. The annealing process was carried out at 1040 °C for 2 h in H₂ flow (500 sccm) under atmospheric pressure to form Cu/Ni alloy foils.

Graphene Growth: Graphene was grown on Cu foil using a low-pressure CVD system, as reported previously.^[31,32] The as-prepared single-crystal Cu foils were placed in a tube furnace and heated to 1020 °C under a 500 sccm flow of Ar. The samples were then annealed for 30 min under a 500 sccm flow of H₂. After the annealing, graphene was grown for 10 min under a 300 sccm flow of H₂ and 0.5 sccm-flow of CH₄.

Characterization: The as-annealed Cu foils were heated at 180 °C on a hot plate for 2–5 min to mildly oxidize the copper foils for initial judgment of single crystal region according to the optical contrast. Moreover, SEM (Thermo Scientific Quattro S), EBSD (AMETEK EDAX DigiView EBSD Camera in combination with EDAX's TEAM, under 20 kV), EDS (AMETEK EDAX Octane Elect EDS System; under 20 kV), AFM (Bruker Dimension Icon with ScanAsyst mode), and transmission electron microscopy (TEM) (FEI Tecnai F30 operated at 300 kV) were employed to analyze the crystal orientation, chemical composition, and surface morphology of as-prepared samples. The cross-sectional specimens of Cu/Ni(510) were fabricated by focus-ion beam milling, in a dual-beam SEM instrument (FEI Strata DB 235).

Supporting Information

Supporting Information is available from the Wiley Online Library or from the author.

Acknowledgements

Y.L.Z.L., L.Z.S., and Z.H.C. contributed equally to this work. The authors thank Ali Cai in Beijing Graphene Institute for designing the geometry of graphite susceptors. They thank Huan Wang in Nankai University for the discussion. They thank Jun Xu and Tao Wang in Electron Microscopy Laboratory, School of Physics, Peking University, for the help on the preparation of cross-sectional specimens and the STEM characterization. They also thank to Beijing National Laboratory for Molecular Science. This work was financially supported by the Beijing Municipal Science & Technology Commission (No. Z181100004818001), the National Basic Research Program of China (No. 2016YFA0200101), the National Natural Science Foundation of China (Nos. 21525310, 51432002, 51520105003, and 11988102).

Conflict of Interest

The authors declare no conflict of interest.

Keywords

anomalous grain growth, Cu foils, high-index facets, single-crystals, strain-engineering

Received: March 24, 2020

Revised: May 12, 2020

Published online: June 11, 2020

- [1] B. Lang, R. W. Joyner, G. A. Somorjai, *Surf. Sci.* **1972**, *30*, 440.
- [2] Y. Hori, I. Takahashi, O. Koga, N. Hoshi, *J. Phys. Chem. B* **2002**, *106*, 15.
- [3] C. Hahn, T. Hatsukade, Y. G. Kim, A. Vaillonis, J. H. Baricuatro, D. C. Higgins, S. A. Nitopi, M. P. Soriaga, T. F. Jaramillo, *Proc. Natl. Acad. Sci. USA* **2017**, *114*, 5918.
- [4] K. Jiang, R. B. Sandberg, A. J. Akey, X. Liu, D. C. Bell, J. K. Nørskov, K. Chan, H. Wang, *Nat. Catal.* **2018**, *1*, 111.
- [5] K. Xia, V. I. Artyukhov, L. Sun, J. Zheng, L. Jiao, B. I. Yakobson, Y. Zhang, *Nano Res.* **2016**, *9*, 2182.
- [6] Y. Hou, B. Wang, L. Zhan, F. Qing, X. Wang, X. Niu, X. Li, *Mater. Today* **2020**, *36*, 10.

- [7] T.-A. Chen, C.-P. Chuu, C.-C. Tseng, C.-K. Wen, H. P. Wong, S. Pan, R. Li, T.-A. Chao, W.-C. Chueh, Y. Zhang, Q. Fu, B. I. Yakobson, W.-H. Chang, L.-J. Li, *Nature* **2020**, 579, 219.
- [8] L. Wang, X. Xu, L. Zhang, R. Qiao, M. Wu, Z. Wang, S. Zhang, J. Liang, Z. Zhang, Z. Zhang, W. Chen, X. Xie, J. Zong, Y. Shan, Y. Guo, M. Willinger, H. Wu, Q. Li, W. Wang, P. Gao, S. Wu, Y. Zhang, Y. Jiang, D. Yu, E. Wang, X. Bai, Z.-J. Wang, F. Ding, K. Liu, *Nature* **2019**, 570, 91.
- [9] A. T. Murdock, A. Koos, T. B. Britton, L. Houben, T. Batten, T. Zhang, A. J. Wilkinson, R. E. Dunin-Borkowski, C. E. Lekka, N. Grobert, *ACS Nano* **2013**, 7, 1351.
- [10] H. I. Rasool, E. B. Song, M. J. Allen, J. K. Wassei, R. B. Kaner, K. L. Wang, B. H. Weiller, J. K. Gimzewski, *Nano Lett.* **2011**, 11, 251.
- [11] H. C. H. Carpenter, *Nature* **1923**, 112, 58.
- [12] Y. C. Cho, S. Lee, M. Ajmal, W. K. Kim, C. R. Cho, S. Y. Jeong, J. H. Park, S. E. Park, S. Park, H. K. Pak, H. C. Kim, *Cryst. Growth Des.* **2010**, 10, 2780.
- [13] Y. Ogawa, B. Hu, C. M. Orofeo, M. Tsuji, K. I. Ikeda, S. Mizuno, H. Hibino, H. Ago, *J. Phys. Chem. Lett.* **2012**, 3, 219.
- [14] B. Deng, Z. Pang, S. Chen, X. Li, C. Meng, J. Li, M. Liu, J. Wu, Y. Qi, W. Dang, H. Yang, Y. Zhang, J. Zhang, N. Kang, H. Xu, Q. Fu, X. Qiu, P. Gao, Y. Wei, Z. Liu, H. Peng, *ACS Nano* **2017**, 11, 12337.
- [15] X. Xu, Z. Zhang, J. Dong, D. Yi, J. Niu, M. Wu, L. Lin, R. Yin, M. Li, J. Zhou, S. Wang, J. Sun, X. Duan, P. Gao, Y. Jiang, X. Wu, H. Peng, R. S. Ruoff, Z. Liu, D. Yu, E. Wang, F. Ding, K. Liu, *Sci. Bull.* **2017**, 62, 1074.
- [16] S. Jin, M. Huang, Y. Kwon, L. Zhang, B. W. Li, S. Oh, J. Dong, D. Luo, M. Biswal, B. V. Cunniff, P. V. Bakharev, I. Moon, W. J. Yoo, D. C. Camacho-Mojica, Y. J. Kim, S. H. Lee, B. Wang, W. K. Seong, M. Saxena, F. Ding, H. J. Shin, R. S. Ruoff, *Science* **2018**, 362, 1021.
- [17] M. C. Desjonquères, D. Spanjaard, C. Barreateau, F. Raouafi, *Phys. Rev. Lett.* **2002**, 88, 561041.
- [18] American Institute of Physics, *American Institute of Physics Handbook* (Ed: D. E. Gray), McGraw-Hill Book Company, New York **1972**.
- [19] X. Xu, D. Yi, Z. Wang, J. Yu, Z. Zhang, R. Qiao, Z. Sun, Z. Hu, P. Gao, H. Peng, Z. Liu, D. Yu, E. Wang, Y. Jiang, F. Ding, K. Liu, *Adv. Mater.* **2018**, 30, 1702944.
- [20] J. Humphreys, G. S. Rohrer, A. Rollett, *Recrystallization and Related Annealing Phenomena*, 3rd ed., Elsevier, Amsterdam, The Netherlands **2017**.
- [21] G. Gottstein, L. S. Shvindlerman, *Grain Boundary Migration in Metal Thermodynamics, Kinetics, Applications*, CRC Press, Boca Raton, FL, USA **2010**.
- [22] R. Carel, C. V. Thompson, H. J. Frost, *Acta Mater.* **1996**, 44, 2479.
- [23] H. J. Frost, C. V. Thompson, D. T. Walton, *Mater. Sci. Forum* **1992**, 94–96, 543.
- [24] C. V. Thompson, R. Carel, *J. Mech. Phys. Solids* **1996**, 44, 657.
- [25] S. H. Kim, S. Z. Han, C. J. Kim, I. Y. Hwang, F. X. Yin, *Mater. Trans.* **2009**, 50, 537.
- [26] H. Wang, X. Xu, J. Li, L. Lin, L. Sun, X. Sun, S. Zhao, C. Tan, C. Chen, W. Dang, H. Ren, J. Zhang, B. Deng, A. L. Koh, L. Liao, N. Kang, Y. Chen, H. Xu, F. Ding, K. Liu, H. Peng, Z. Liu, *Adv. Mater.* **2016**, 28, 8968.
- [27] E. M. Zielinski, R. P. Vinci, J. C. Bravman, *J. Appl. Phys.* **1994**, 76, 4516.
- [28] T. Wu, X. Zhang, Q. Yuan, J. Xue, G. Lu, Z. Liu, H. Wang, H. Wang, F. Ding, Q. Yu, X. Xie, M. Jiang, *Nat. Mater.* **2016**, 15, 43.
- [29] M. Huang, M. Biswal, H. J. Park, S. Jin, D. Qu, S. Hong, Z. Zhu, L. Qiu, D. Luo, X. Liu, Z. Yang, Z. Liu, Y. Huang, H. Lim, W. J. Yoo, F. Ding, Y. Wang, Z. Lee, R. S. Ruoff, *ACS Nano* **2018**, 12, 6117.
- [30] J. Li, Y. Li, J. Yin, X. Ren, X. Liu, C. Jin, W. Guo, *Small* **2016**, 12, 3645.
- [31] L. Sun, L. Lin, J. Zhang, H. Wang, H. Peng, Z. Liu, *Nano Res.* **2017**, 10, 355.
- [32] L. Sun, L. Lin, Z. Wang, D. Rui, Z. Yu, J. Zhang, Y. Li, X. Liu, K. Jia, K. Wang, L. Zheng, B. Deng, T. Ma, N. Kang, H. Xu, K. S. Novoselov, H. Peng, Z. Liu, *Adv. Mater.* **2019**, 31, 1902978.